ResearchGate

See discussions, stats, and author profiles for this publication at: https://www.researchgate.net/publication/236234610

Ordering of Gold Nanorods in Confined Spaces by Directed Assembly

ARTICLE *in* MACROMOLECULES · MARCH 2013

Impact Factor: 5.8 · DOI: 10.1021/ma400115z

CITATIONS
26

READS
61

10 AUTHORS, INCLUDING:

Peng Zhang
Tianjin University
25 PUBLICATIONS **401** CITATIONS
SEE PROFILE

Jie He
University of Connecticut
52 PUBLICATIONS **1,104** CITATIONS
SEE PROFILE

Renhua Deng
Huazhong University of Science and Technology
26 PUBLICATIONS **325** CITATIONS
SEE PROFILE

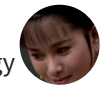

Ming-Hui Lu
Nanjing University
91 PUBLICATIONS **1,988** CITATIONS
SEE PROFILE

Available from: Renhua Deng
Retrieved on: 28 January 2016

Macromolecules

Article

pubs.acs.org/Macromolecules

Ordering of Gold Nanorods in Confined Spaces by Directed Assembly

Weikun Li,[†,‡] Peng Zhang,[‡] Ming Dai,[§] Jie He,[‡] Taarika Babu,[‡] Ye-Long Xu,[§] Renhua Deng,[†] Ruijing Liang,[†] Ming-Hui Lu,[§] Zhihong Nie,*[,‡] and Jintao Zhu*[,†]

[†]Key Laboratory of Large-Format Battery Materials and System, Ministry of Education, School of Chemistry and Chemical Engineering, Huazhong University of Science and Technology, Wuhan 430074, P. R. China

[‡]Department of Chemistry and Biochemistry, University of Maryland, College Park, Maryland 20742, United States

[§]National Laboratory of Solid-State Microstructures and Department of Materials Science and Engineering, Nanjing University, Nanjing 210093, P. R. China

Supporting Information

ABSTRACT: This paper describes an effective approach to order gold nanorods (NRs) within cylindrically confined microdomains of block copolymer- (BCP-) based supramolecular assemblies. Individual BCP micelles encapsulated with well-ordered NRs can be obtained by disassembling the supramolecular structures. The mismatch of binary polymer brushes with different lengths on the surface of the NRs was used to effectively improve the dispersion of the NRs within polymer matrix, due to enhanced wetting of the brushes by surrounding mismatch polymers. This enables us to quantitatively explore the location and orientation of the NRs within confined geometries. By varying the content of NRs, the aspect ratio of the NRs, or the diameter of the cylindrical BCP micelles, the orientation of the NRs within micelles can be tuned to form one-dimensional nanostrings with end-to-end organization of NRs along the micelles or with side-by-side twisted arrangement of NRs perpendicular to the micelles. UV−vis spectroscopy measurements and finite-difference time-domain (FDTD) calculations confirm that our approach provides a simple yet versatile route to tune the optical properties of the hybrid micelles by controlling the ordering of the NRs. This work provides guidelines for dispersing other functional anisotropic NPs, and lays groundwork for the fabrication of optical and electronic devices.

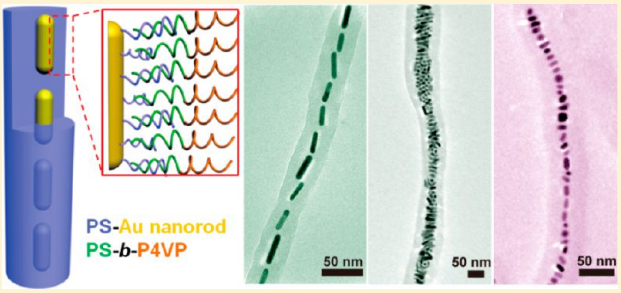

1. INTRODUCTION

Controlled assembly of inorganic nanoparticles (NPs) within a polymer matrix creates novel nanocomposites with enhanced mechanical, optical, electric, and magnetic properties,[1−4] facilitating their applications in the fields of sensing, catalysis, bioimaging, drug delivery, and optical and electronic devices.[5] In particular, nanorod (NR)−based nanocomposites have attracted tremendous interests primarily because of the unique inherent physical properties originated from the one-dimensional shape of NPs.[6−9] For example, the plasmonic properties of Au NRs can be tuned by simply varying the aspect ratio of the NRs. To enhance the performance of the composites, it is critical to control the spatial arrangement of individual anisotropic NRs within the polymer hosts with high precision. Several attempts have been established to assemble NRs, including template or external fields mediated assembly,[10,11] stretching of polymer films,[12,13] among others.[14,15] In particular, incorporation of the NRs within or on the surface of homopolymer[16,17] and block copolymer (BCP) films[18−23] have attracted enormous attention.

Despite considerable progress in the field,[24,25] it remains a challenge to control the arrangement (namely, distribution and orientation) of NRs in polymeric matrix, because the NRs tends to aggregate side-by-side due to the interactions including the depletion forces, van der Waals and the dipole−dipole interactions. To avoid aggregation and to control their spatial arrangement of NRs in the polymer matrix, one must reduce rod−rod attraction and employ strong favorable interactions between the NRs and the host polymers to offset the entropic penalty associated with this process. A commonly used method is to functionalize NRs with polymer brushes that favorably interact with polymer host and reduce the rod−rod attractive interactions. Also, the uniform dispersion of NRs in polymer matrix is mainly determined by whether the brushes on the NRs are wetted by the matrix polymer. Theoretical and experimental studies demonstrate that NRs can be dispersed well in polymer matrix only when the molecular weight (M_w) of matrix polymers is similar to or smaller than the M_w of the brushes. Yet, even when the brushes are chemically identical to the matrix, an unfavorable entropic interaction still remains, due

Received: January 17, 2013
Revised: February 22, 2013
Published: March 5, 2013

 © 2013 American Chemical Society dx.doi.org/10.1021/ma400115z | Macromolecules 2013, 46, 2241−2248

to the so-called "autophobic dewetting" effect.[26−28] In contrast to polymer brushes on a planar substrate, the surface wettability of polymer brushes on NPs by matrix polymers strongly depends on the surface curvature of NPs and the relative length of polymer brushes to the size of NPs. Given a constant grafting density of polymers on NPs, NPs with larger surface curvature provide more void space between the terminals of polymer brushes on NPs, thus enhancing the wettability of the NPs.[29] Thus, compared to spherical NPs, the relatively small surface curvature of the longitudinal side of NRs makes them more difficult to disperse in polymer matrix due to insufficient conformational freedom for the matrix polymers close to the NR surface. We hypothesize that the use of binary polymer brushes with different lengths as ligands will improve the wettability of NRs and thus the uniform dispersion of NRs within polymer matrix by creating additional void spaces close to the NR surface. This assumption is consistent with recent theory predictions that a bimodal polymer brush on the planar substrate can suppress "autophobic dewetting" effect.[30]

This paper reports a simple strategy to control the dispersion and orientation of NRs within BCP micelles by grafting a binary polymer brushes on the surface of NRs. We show that gold NRs tethered of polystyrene (PS) with bimodal chain length can be effectively incorporated into cylindrical PS domain of PS-*b*-poly(4-vinylpyridine) (PS-*b*-P4VP) through the directed supramolecular assembly. Individual hybrid micelles can be obtained by disassembly of the supramolecules. By tuning three experimental parameters, including the diameter of the cylindrical BCP micelles, the aspect ratio of the NRs, and the content of the NRs (e.g., volume fraction of NR: φ_{NR}) added, NRs can be uniformly dispersed into the core of the micelles with parallel or perpendicular orientation (Figure 1). When φ_{NR} is low, the NRs organize end-to-end to form nanostrings, and the length of the strings gradually increases with an increase in the φ_{NR}. When φ_{NR} increases above ∼20 vol %, the organization of the NRs transits to side-by-side mode. The highly ordered arrays of gold NRs with a close inter-rod spacing allows the control over the plasmon properties of the ensemble of gold NRs. End-to-end assembly of NRs leads to a red shift in the longitudinal surface plasman resonance (SPR), while side-by-side alignment shows a blue shift. This general and straightforward approach can be potentially applied to assemble other anisotropic NPs (i.e., cube or octahedron) into new functional composite materials with unique optical and electronic properties or new collective properties.[31]

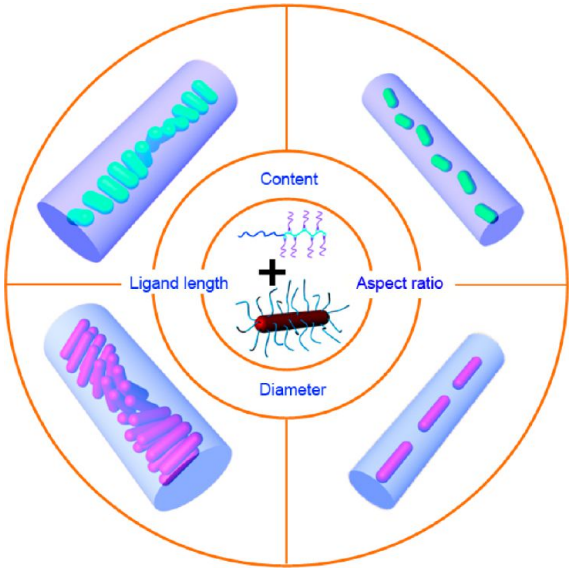

Figure 1. Schematic illustration showing the various ordered NRs arrangements encapsulated within discrete cylindrical micelle via directed supramolecular assembly. Gold NRs grafted with binary PS brushes with different chain length were selectively incorporated into the PS cylindrical domains of supramolecules PS-*b*-P4VP(PDP)$_x$. Discrete cylindrical micelle encapsulated with NRs was obtained through disassembly of the supramolecules, and the orientation of the NRs in the cylinders can be effectively tailored by varying the diameter of the micelles, the aspect ratio of the NR, or the NRs content.

2. EXPERIMENTAL SECTION

Materials. Sodium borohydride ($NaBH_4$), Ascorbic acid, Hydrogen tetrachloroaurate trihydrate ($HAuCl_4{\cdot}3H_2O$, purity: 99.999%), $AgNO_3$, 3-*n*-Pentadecylphenol (PDP, purity: 97%, recrystallized twice from *n*-hexane before used) and cetyltrimethylammonium bromide (CTAB, purity ≥99%) were obtained from Sigma-Aldrich. PS_{20k}-*b*-$P4VP_{17k}$ (PDI = 1.08), PS_{51k}-*b*-$P4VP_{18k}$ (PDI = 1.15), PS_{110k}-*b*-$P4VP_{107k}$ (PDI = 1.15), PS_{2k}-SH (PDI = 1.15), PS_{5k}-SH (PDI = 1.4), PS_{12k}-SH (PDI = 1.09), PS_{20k}-SH (PDI = 1.07), and PS_{50k}-SH (PDI = 1.06) were purchased from Polymer Source, Inc., Canada. Deionized water (Millipore Milli-Q grade) with resistivity of 18.0 MΩ was used in all the experiments. All the glassware were cleaned by aqua regia and rinsed with deionized water prior to the experiments.

Gold NRs Synthesis. Gold NRs with longitudinal SPR of more than 800 nm were synthesized following the published protocols.[32] The seed solution of gold NRs was prepared by reducing $HAuCl_4$ (2.5 mL, 1 mM) mixed with 5 mL of a 0.2 M aqueous solution of CTAB, 2.5 mL deionized H_2O and fresh sodium borohydride (0.6 mL, 10 mM) in ice-cold water. For the preparation of a growth solution, 19 mL of a 0.1 M CTAB solution was mixed with 1 mL of a 10 mM aqueous solution of $HAuCl_4$, 0.2 mL of 10 mM aqueous solution of $AgNO_3$. Followed by the addition of 0.12 mL of 0.1 M aqueous solution of ascorbic acid, the dark yellow solution turned colorless. Finally, 0.32 mL of a 5-min-aged seed solution of NPs was added to the growth solution. The NRs were purified using twice 30-min-long centrifugation cycles at 10 000−12 000 rpm. At the end of each centrifugation cycle, the supernatant was removed and the precipitated NRs were redispersed in deionized water.

Gold NRs with longitudinal SPR of less than 700 nm were synthesized following published approach.[33] The short NRs were synthesized by the oxidation method, e.g., adding 0.5 mL of H_2O_2 (35 wt %) into the 20 mL starting Au NRs (longitudinal SPR of more than 800 nm) solution. The oxidation process was monitored by UV−vis spectroscopy. The resulting mixtures were kept at 23 °C for 2 h before the separation process. We note that the reaction time for the short Au NRs fabrication depends strongly on the reaction temperature.

Surface Modification of Gold NRs. Entire surface of Au NRs were modified by PS-SH through the two-step ligand-exchange approach.[34,35] In a typical experiment, approximately 0.4 mL of the concentrated (∼0.8 mg/mL) aqueous solution of NRs was added to 10 mL of a 0.2 mg/mL solution of PS_{12k}-SH in THF. The solution was sonicated for 30 min and incubated for at least 24 h. The modified NRs were washed with $CHCl_3$ three times to remove CTAB and free PS-HS, and then the precipitate was dissolved in 4 mL chloroform. Purification procedure was performed by using three 30-min-long centrifugation cycles at 10 000−12 000 rpm. Furthermore, PS-SH (4 mg PS_{12k}-SH and 1 mg PS_{2k}-SH) in chloroform was added to the resulting PS-coated Au NRs solution, followed by the same sonication, incubation, and purification process as carried out above. Finally, Au NRs with high grafting density were thus obtained (see the Supporting Information, Table S1). Au NRs were very stable in THF and no significant change was found by dispersing the NRs in THF for two months. NRs core diameter and overall length obtained from TEM image analysis was used to calculate the average surface area per NR.

dx.doi.org/10.1021/ma400115z | *Macromolecules* 2013, 46, 2241−2248

PS graft density on the NR surface was estimated based on average particle size from TEM images and SEM results (see Supporting Information, Table S1), assuming ρ_{gold} = 19.3 g/cm^3 and ρ_{PS} = 1.05 g/cm^3.[36]

Generally, increasing the molecular weight of the brush can suppress the autophobic dewetting, and usually decrease the rods−rods interaction due to increase of steric hindrance. Besides using PS_{5k}, PS_{12k}, PS_{20k}, PS_{50k}, and the mixtures of PS_{2k} and PS_{12k} (PS_{2k}: PS_{12k} = 1:1), we also tried to modify the NRs with neat short ligand PS_{2k}. Unfortunately, the PS_{2k}-grafted NRs are unstable in THF and form aggregates after the first modification step.

Preparation of PS-*b*-P4VP/NRs Hybrid Micelles. PS-*b*-P4VP and PDP were separately dissolved in chloroform to form 1 wt % solutions. Then, the solutions were mixed together at stoichiometric amount of PDP according to the number of pyridine groups in P4VP, followed by stirring two days to complete the hydrogen bonding. Subsequently, PS-coated Au NRs in chloroform was added to the PS-*b*-P4VP(PDP) solution. The resulting solution was then stirring for 5 min. Slow evaporation of chloroform gave rise to hybrid sample film, followed by solvent annealing under saturated chloroform atmosphere at room temperature over 12 h before drying in vacuum for 6 h.[35,37] Finally, ∼ 0.5 mg of the hybrid micelles was dispersed in ethanol and dialyzed against ethanol by using dialysis tubing (DM27 EI9004, USA; cutoff 12 000−14 000).

Characterization. Transmission electron microscopy (TEM) investigation was performed on a JEOL 2100 LaB6 or FEG TEM operated at an acceleration voltage of 200 kV. HAADF-STEM was performed using an FEI Magellan 400 FESEM in STEM mode equipped with the HAADF detector. To prepare samples for TEM, a small drop of the aqueous solution containing hybrid micelles was placed on 300 mesh copper grids covered with carbon film, and water was subsequently evaporated. To increase the contrast for the samples, the hybrid micelles were stained by subsequently adding a drop of 0.5 wt % phosphotungstic acid (PTA) in aqueous solution to the TEM grid.[38] Scanning electron microscopy (SEM) (Sirion 200, FEI) investigation was operated at voltage of 10 kV. Samples for SEM were prepared by casting one drop of the hybrid micellar solution on silicon wafers, and dried at room temperature. For UV−vis spectroscopy investigation, hybrid micelles in ethanol solution after dialysis was placed in quartz sample cell. Absorption spectra (ranged from 400 to 1100 nm) were recorded by using LAMBDA 45 UV−vis spectraphotometer (Perkin-Elmer) at 25 °C with reference spectrum of anhydrous ethanol.

Finite-Difference Time-Domain (FDTD) Simulations. We also performed FDTD calculations to investigate the variation of scattering spectrum with the formation of NRs assemblies. The FDTD calculations were performed by using FDTD Solutions 8.0, which was developed by Lumerical Solutions, Inc. During the calculations, an electromagnetic pulse in the wavelength range from 400 to 1500 nm was launched into a box containing the target Au NR chain to simulate a propagating plane wave. The Au NR chain is surrounded by a PS cladding. The source type is total-field scattered-field sources (TFSF). The Au NRs chain and its surrounding space were divided into 0.5 nm meshes. The NR was modeled as a cylinder and its size was set to be in the range of size measured from the experiment. The radius and the length are 3.6 and 25 nm, respectively. And gap for side-by-side and end-to-end is 3.1 and 8 nm. And the rod number for them is 4 and 5, respectively. Refractive index of the substrate is 1.58 to simulate PS and that of medium is 1.33 to simulate water. The dielectric function of gold was represented with a Drude model:

$$\varepsilon(\omega) = \varepsilon_\infty - \frac{\omega_p^2}{\omega^2 + i\gamma\omega} \quad (1)$$

The parameters in above equation are the high-frequency dielectric constant ε_∞ = 10, the plasma frequency ω_p = 1.37 × 10^{16} rad/s, and the Drude damping constant γ = 5 × 10^{14} rad/s. The different excitation polarizations were considered by setting the electric field being parallel or perpendicular to the NR length axis. The field distributions were obtained at the different resonance modes. Five NRs were considered for the end-to-end simulation and four NRs were considered for the side-by-side simulation.

3. RESULTS AND DISCUSSION

3.1. New Strategy to Disperse and Orient Gold NRs in Confined Spaces. We used supramolecular assembly route to direct gold NRs into cylindrical micelles, as illustrated in Figure 1. Generally, PS-*b*-P4VP and 3-*n*-pentadecylphenol (PDP) would form PS-*b*-P4VP(PDP)$_x$ (the subscript x represents the ratio of PDP to PVP units) comb−coil supramolecules which can further assemble into hierarchical structures. We generated cylindrical PS structures dispersed in P4VP(PDP) matrix by controlling PDP content in the PS_{51k}-*b*-$P4VP_{18k}(PDP)_{2.0}$ (volume fraction of PS φ_{PS} = 23 vol %) supramolecules. Monodisperse gold NRs with diameter of 7.2 ± 1.0 nm and length of 28.9 ± 3.9 nm were synthesized by the seeding growth approach (Figure S1, Supporting Information).[32,36] Short gold NRs with diameter of 6.2 ± 1.2 nm and length of 12.6 ± 2.5 nm were synthesized via H_2O_2 oxidation of the long gold NRs (Figures S2 and S3, Supporting Information).[33] The original gold NRs were transferred into organic solvents by grafting thiol-terminated PS_{12k}. These gold NRs were subsequently functionalized by mixed brushes of long (PS_{12k}) and short (PS_{2k}) PS through a two-step ligand-exchange approach.[35,39] The grafting density of PS on the surface of the gold NRs was estimated to be about 1.27 chains/nm^2 (calculated for PS_{12k}), which is comparable to the value reported for spherical Au NPs (Table S1, Supporting Information).[35] PS_{2k} and PS_{12k}-grafted NRs were successfully incorporated into PS domains of PS-*b*-P4VP(PDP)$_{2.0}$ assemblies due to the improved wettability of the PS brush on surface of NRs with PS block. Because of the reversible nature of the hydrogen bonding between phenol group of the PDP and 4-vinylpyridine units of P4VP, the formed hierarchical microstructures can be disassembled into isolated micelles with PS-core and P4VP-shell when P4VP(PDP) phase forms the matrix. Thus, isolated cylindrical micelles with uniformly dispersed gold NRs were obtained upon the breakdown of the hydrogen bonding (Figure 2).

We note that the polymer brush on the NRs plays an important role in the dispersion of NRs in the cylindrical micelles. To explore the wetting behavior of polymer brush with the matrix polymer, we first grafted only a single type of polymer brush on the NRs, e.g., thiol-terminated PS with molecular weights of 5k, 12k, 20k, or 50k (referred to as PS_{5k}, PS_{12k}, PS_{20k}, and PS_{50k})(see Table S2, Supporting Information). As shown in Figure 3a, when PS_{5k} grafted NRs were employed, the NRs preferentially assembled side-by-side to form an ordered smectic B phase (see Figure S4a, Supporting Information, for low-magnification SEM). We attributed the formation of ordered smectic structures to the following reasons: (1) Because of the high grafting density of PS brush on the surface of NRs, PS_{51k} block of the copolymer is hard to penetrate into the dense PS_{5k} brush on the NRs. The interaction between matrix polymer and the brush is weak, while the interaction between NRs and NRs is strong. (2) Autophobic dewetting occurs because of the large mismatch between the brush molecular weight (PS_{5k}) and that of the PS_{51k} block. The same phenomena were also observed when PS_{12k} and PS_{20k} brushes were used. In the case of PS_{12k}-grafted NRs, NRs were directed into the end-cap of the micelles and formed bundles (Figure 3, parts c and d, and Figure S4b (Supporting Information) for low-magnification TEM image).

dx.doi.org/10.1021/ma400115z | Macromolecules 2013, 46, 2241−2248

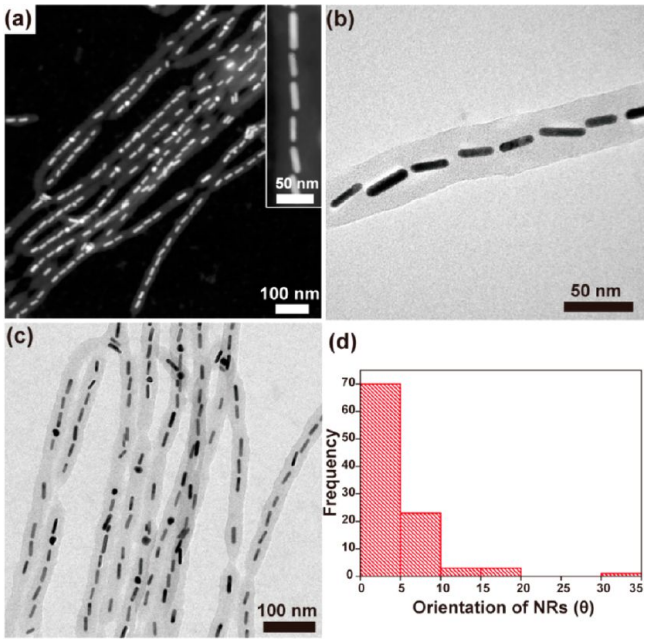

Figure 2. TEM images of cylindrical PS_{51k}-*b*-$P4VP_{18k}$ micelles encapsulated with 16 vol % binary PS brushes (mole ratio of PS_{2k}: PS_{12k} = 1:1) grafted NRs (diameter: 7 nm; length: 29 nm). Key: (a) low-magnification and inset high-magnification dark-field TEM images; (b, c) high-magnification bright-field TEM images of PS_{51k}-*b*-$P4VP_{18k}$ micelles with PS-NRs encapsulated; (d) histogram showing the orientation of the NRs with respect to the axis of cylindrical micelle.

Further increasing the brush molecular weight to PS_{50k} which is comparable to the chain molecular weight of the copolymer (PS_{51k}, shown in Figure 3, parts e and f), the NRs can disperse well in the PS_{51k} microdomains. Interestingly, the initial cylindrical micelles turned into spherical structures (see Figure S4c, Supporting Information, for low-magnification TEM). The BCPs act as a template to direct NP arrangement, while the NPs induce phase transitions of the BCPs.[35,40] However, this result is opposite to our expectation that a morphological transition from cylindrical to nanosheet structures should occur due to the increased volume fraction of PS (φ_{PS}) as NRs addition. Such transition from cylinders to spheres is still unclear and needs to be further investigated. We presume that this phase transition is mainly a result of entropic penalty associated with chain stretching around larger NRs coated with long PS. This effect is less significant for NRs coated with short PS.[41]

The dispersion efficiency of the NRs was significantly enhanced when NRs were modified with binary brushes of PS_{12k} and PS_{2k} on their surfaces (Figure 2a–c). NRs were selectively self-assembled into the PS domains of the BCPs. Figure 2a shows a dark-field TEM image of the hybrid cylindrical micelles with NRs uniformly dispersed in the core over a long distance (up to ~0.5–6 μm in length). The NRs are aligned parallel to the long axis of the cylindrical micelle, in order to minimize the entropic deformation of the BCPs and to overcome the rod–rod interaction (dipole–dipole and van der Waals interaction). The NRs organized end-to-end to form nanostrings within the cylinders, which is consistent with computational results by Chen et al.[42] We note that the incorporation of NRs does not significantly change the overall cylindrical morphologies (Figure 2c). To quantitatively understand the assembly process, we define the orientation of the NRs with respect to the long axis of cylindrical micelle as θ. Clearly, θ was within 10° for 90% of the NRs in the cylinder, indicating the parallel nature of the NRs to the cylindrical micelles (Figure 2d).

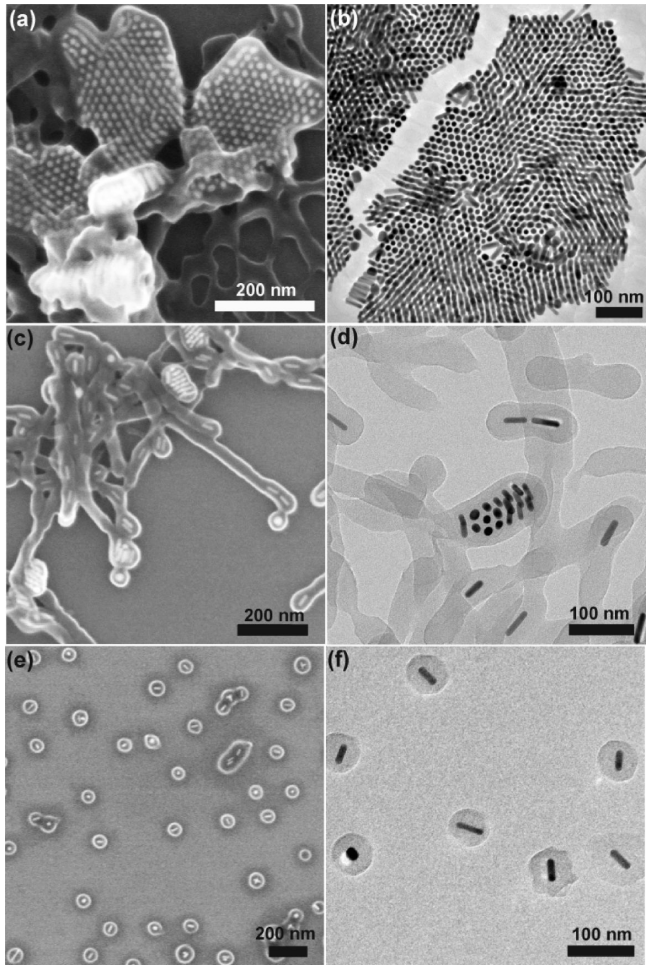

Figure 3. SEM images (a, c, e) and bright-field TEM images (b, d, f) of the hybrid micelles formed from PS_{51k}-*b*-$P4VP_{18k}(PDP)_{2.0}$ and 10 vol % NRs (diameter: 7 nm; length: 29 nm) grafted with PS of different molecular weight: (a, b) PS_{5k}; (c, d) PS_{12k}; (e, f) PS_{50k}.

3.2. Tuning the Length of the NR Strings. The ability to tune the length of the NR strings as well as the inter-rod spacing provides an additional strategy to tailor the plasmonic coupling between NRs, thus the collective optical properties of assemblies.[6,36,43–45] The string length can be effectively tuned by simply varying φ_{NR} (diameter: 7.2 ± 1.0 nm; length: 28.9 ± 3.9 nm) (Figure 4). Parts a–c of Figure 4 display the TEM images of the hybrid cylindrical micelles for 3.5 vol %, 8 vol % and 16 vol % NR loading (also see Table S3, Supporting Information). The NRs were dispersed homogeneously within the cores of the cylindrical micelles in a single line (see Figure S5, Supporting Information, for low-magnification SEM and TEM). The length of the NR strings increased from 50 ± 20 nm to 304 ± 171 nm when φ_{NR} increased from 3.5 vol % to 16 vol %, as shown in Figure 4e (also see Figure S6, Supporting Information, for the histograms of the length of the NRs strings distribution). However, the inter-rod spacing remained nearly constant at 5.3 ± 2.7 nm when φ_{NR} was increased up to 16 vol %. The standard deviation of the nanostring length increased significantly due to increased loading of the NRs. Compared

dx.doi.org/10.1021/ma400115z | *Macromolecules* 2013, 46, 2241–2248

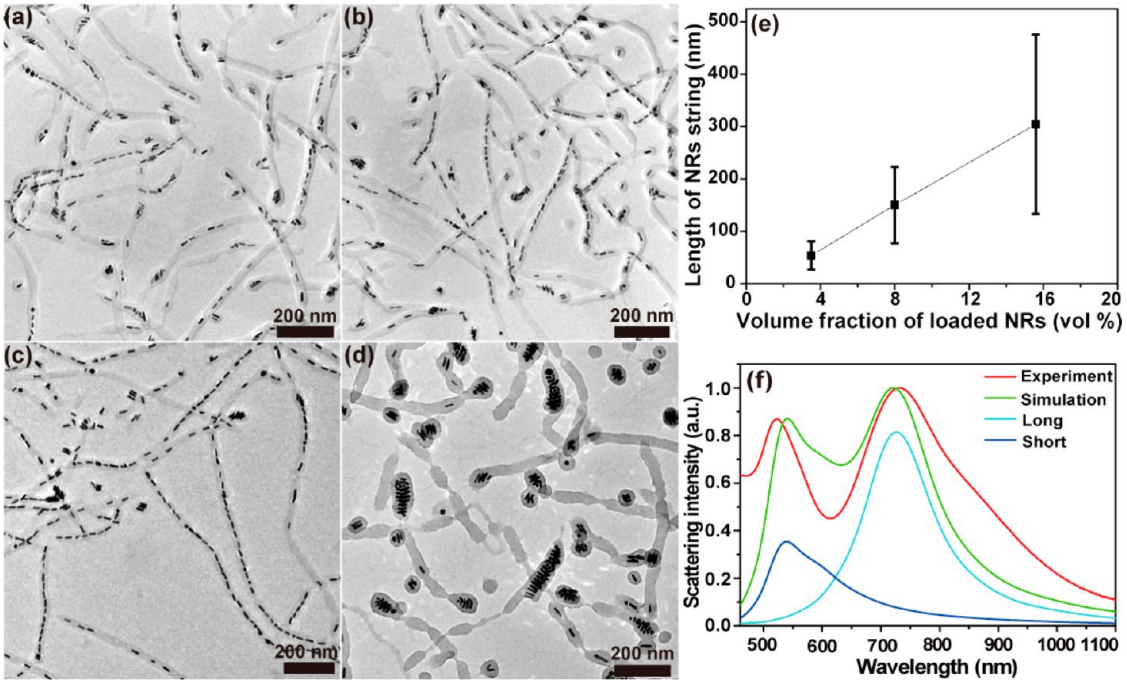

Figure 4. (a–d) Bright-field TEM images of cylindrical micelles encapsulated with gold NRs (diameter: 7 nm; length: 29 nm) grafted with mixed PS brushes (PS_{2k}:PS_{12k} = 1:1), formed from PS_{51k}-*b*-$P4VP_{18k}(PDP)_{2.0}$ with different NRs content: (a) 3.5 vol %; (b) 8 vol %; (c) 16 vol %; (d) 27 vol %. Accordingly, the diameter of the hybrid micelles increased from 32 to 41 nm when increasing NRs loading from 3.5 to 16 vol %. (e) Plot of the length of the nanostring of NRs as a function of φ_{NR} in the composite. (f) Experimental UV–vis (red line) and calculated scattering spectra (green line) of the hybrid micellar solution with NRs content of 27 vol % (NRs form side-by-side bundles). The blue and cyan curves represent the short-wave (540 nm) and long-wave (721 nm) resonance of side-by-side assemblies of four Au NRs in PS with an inter-rod spacing of 3.1 nm. For comparison, the experiment value of the two resonances is 524 and 730 nm, respectively.

with isolated NRs before assembly, the longitudinal SPR spectra of the hybrid micelles red-shifted up to 75 nm with an increase in the nanostring length (Figure 5). Further increasing

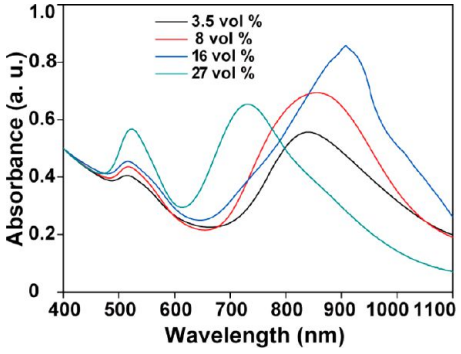

Figure 5. UV–vis spectra of the hybrid micelles solution with different NRs contents. The cylindrical micelles, encapsulated with gold NRs (diameter: 7 nm; length: 29 nm) grafted with mixed PS brushes (PS_{2k}:PS_{12k}= 1:1), were formed from PS_{51k}-*b*-$P4VP_{18k}(PDP)_{2.0}$ with different NRs content: (a) 3.5 vol %; (b) 8 vol %; (c) 16 vol %; (d) 27 vol %.

the φ_{NR} above ~20 vol % led a transition of NR alignment from end-to-end to side-by-side mode in assemblies (Figure 4d). In this case, NRs stacked side-by-side to form cross-like structure due to the steric constraints between NRs inside the cylindrical micelles. The number of NRs per aggregates ranged from ~3 to 40 (see Figure S7, Supporting Information, for low-magnification SEM and TEM). Compared to the end-to-end assembly of the NRs, the inter-rod spacing in the side-by-side bundles was decreased to 3.1 ± 0.5 nm. Accordingly, the assemblies exhibited a 103 nm blue-shift in the longitudinal SPR and a 14 nm red-shift in the transverse plasmon band (Figure 5), when the cross-like stacking structure occurred.[46] Significantly, the FDTD simulation of the plasmonic peaks of the assemblies agrees qualitatively with our experiment data (as shown in Figures 4f, 5, and S8 (Supporting Information)). The experimental value of the two resonances is 908 and 516 nm, while the simulation value is 930 and 499 nm. In short, at a low φ_{NR} (e.g., lower than 20 vol %), NRs adopt end-to-end mode to form nanostrings with NRs parallel to the axis of the cylinders, in order to minimize the polymer conformation entropy due to the unfavorable deformation of the PS chains surrounding the NRs. As φ_{NR} increases, the rod–rod interactions overcome the energetic penalty associated with deforming BCP cylindrical microdomains, thus leading to the formation of cross-like stacking structure.[23] Our method, therefore, provides an easy means to control the length of the NRs chains and orientation of NRs in micelles, thus facilitating their subsequent function in color polarizing filters, photovoltaic, and high-density optical data storage.[47]

3.3. NRs Dimension Effect on Their Ordering in Confined Spaces. The dimension of the NRs plays an important role in their dispersion and orientation in polymer host. The associated free-energy penalty between the NRs and the polymer matrix during the self-assembly can be given by:

$$\Delta F \sim \frac{3}{2} kT(L'^2 - L^2)/{R_0}^2 + \gamma \, dA \qquad (2)$$

where k is Boltzmann constant, T is temperature, and dA and γ are the variation in interfacial area and interfacial tension, L and L' is the domain thickness before and after the addition of

dx.doi.org/10.1021/ma400115z | *Macromolecules* 2013, 46, 2241–2248

NRs.[48] Therefore, the increase in NR size not only increases the conformation entropy of the polymer $(3/2k(L'^2 - L^2)/R_o^2)$ but also causes the enthalpical incompatibility.[49] To explore the influence of NR aspect ratio on the assembly morphology, we tested short gold NRs with a small aspect ratio of 2.0 (diameter: 6.2 ± 1.2 nm, length: 12.6 ± 2.5 nm) at NRs loading of 11 vol % and 21 vol %. NRs distributed homogeneously within the core of cylindrical micelles when short gold NRs were used (Figure 6, parts a and c). Orientation of the NR, θ, is within

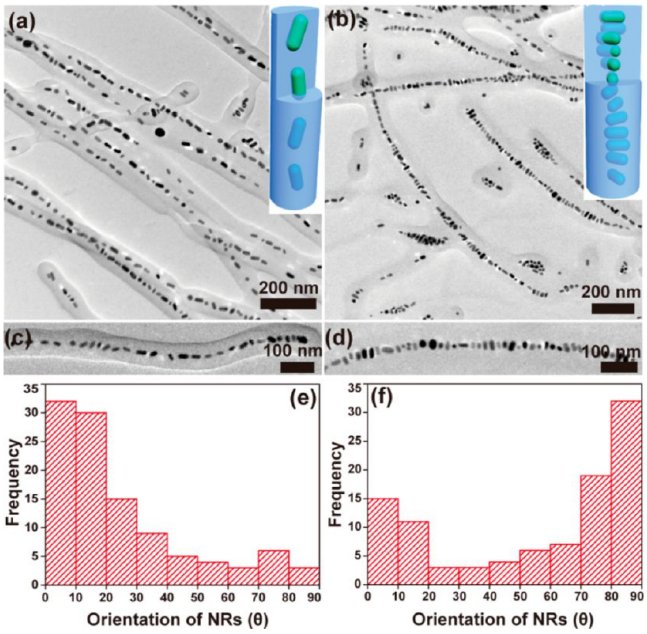

Figure 6. (a, b) Bright field TEM images of hybrid cylindrical micelles formed from PS_{51k}-*b*-$P4VP_{18k}$ $(PDP)_{2.0}$ with varied NRs (diameter, 6 nm; length, 12 nm) content: (a, c) 11 vol %; (b, d) 21 vol %. The NRs were grafted with binary PS brushes (PS_{2k}:PS_{12k} = 1:1). Inset in the upper-right shows the orientation of NRs in the cylinders. (e, f) corresponding histogram showing the orientation of the NRs in the hybrid cylindrical micelles.

±20° and ±40° for 60% and 85% of the NRs, respectively, indicating the parallel nature of the NRs to the long axis of the cylinders (Figure 6, parts b and d, also see the histograms of the length and inter-rod distance in Figure S9, Supporting Information).

We used the pressure $P(z)$ due to PS brush acting at a z position away from the PS/P4VP interface ($z = 0$) to interpret the orientation of NRs within the polymer matrix (see Scheme S1, Supporting Information). The $P(z)$ is given by:[21,50]

$$P(Z) = \frac{3\pi^2 h^2}{8N^2 b^5}\left(1 - \frac{z^2}{h^2}\right) \quad (3)$$

where h is the height of the PS brush ($2h = D_{Diameter\ of\ micelles}$), N is degree of polymerization of the PS and b is the statistical segment length. To estimate the orientation change of the NRs due to varied aspect ratio, we assume that h does not alter with the addition of different NRs in the PS domain and NRs bear the same pressure $P(z)$ condition at the highest point, such that $\sin\theta = 2(h - z)/L$, where θ is the orientation of the NRs and L is the length of the NRs. One can predict the relationship between the length L and the orientation θ of NRs using this simple equation. For the long NRs (L is 28.9 nm), θ is within 10°, and $h - z$ is about 2.5 nm. In the case of short NRs, θ is estimated to be 23° if we assume that the $h - z$ does not change. This calculated value is consistent with our experimental result that about 60% of the short NRs oriented within ±20° (Figure 6, parts a and e). Clearly, orientation freedoms of the NRs are strongly restricted in order to minimize the entropic penalty associated with the deformation of the PS chains around NRs when the length of NRs is increased due to the confinement from the cylinders. Similarly, short NRs underwent morphological transition during assembly; and they assembled homogeneously side-by-side within the cylindrical micelles once φ_{NR} is above ~20 vol % (see Figure 6b and Figure S9, Supporting Information). In this case, about 50% of the NRs are oriented within 80–90°, perpendicular to the axis of the cylinders (Figure 6f).

3.4. Effect of the Dimension of the Host Micelles on the NRs Ordering. To determine the influence of diameter of cylindrical micelles on the assembly morphology, we compared three kinds of BCP-based supramolecules of PS_{20k}-*b*-$P4VP_{17k}(PDP)_{1.0}$ (φ_{PS} = 23 vol %), PS_{51k}-*b*-$P4VP_{17k}$ $(PDP)_{2.0}$ (φ_{PS} = 30 vol %), and PS_{110k}-*b*-$P4VP_{107k}$ $(PDP)_{1.0}$ (φ_{PS} = 30 vol %) (Figure S10, Supporting Information) at a fixed NRs loading of 16 vol %. When PS_{20k}-*b*-$P4VP_{17k}(PDP)_{1.0}$ (mean-square end-to-end distance (R_0) of the PS_{20k}: 9.3 nm) and NRs (diameter: 7.2 nm) were used, NRs behave like a big hairy particle (or homopolymer with huge molecular weight) which can significantly swell the PS domains. In this case, monodisperse spherical micelles (~90%) loaded with one NR for each were observed, as shown in Figure 7, parts a and b (also see Figure S11a, Supporting Information). Increasing molecular weight of PS to 51k (R_0 of the PS_{51k}, 15.1 nm; $D_{micelles}$, 32 nm) led to the formation of cylindrical hybrid micelle with incorporated NRs parallel to the long axes of the cylinders (Figure 7, parts c and d). Further increase of the diameter of cylindrical micelle (for PS_{110k}-*b*-$P4VP_{107k}$, R_0 of the PS_{110k}, 22.2 nm, $D_{micelles}$, 86 nm) gave rise to hybrid micelles with side-by-side assembled NRs perpendicular to their long axis (Figure 7, parts e and f). It is interesting that the NRs self-assembled into hexagonal arrangement within the cylinders. The assemblies twisted along the cylindrical axis in order to further release polymer conformation entropy and the excluded volume of the polymer at the end of the NRs (Figure S11b, Supporting Information).[51] However, we are not sure whether the twisted assemblies are helical or not. Hexagonally arranged helical NRs structure has been reported by Glotzer and co-workers through computer investigations.[51−53] Similar results were obtained when short NRs were directed into the cylindrical micelles with varied diameters, as shown in Figure S12, Supporting Information. To the best of our knowledge, this is the first example of the formation of hexagonal cylinder phase with a twist along the cylindrical axis in the polymer film. Further improvement of the uniformity of the gold NRs may lead to the formation of helical structures.[54] The new assembled structures may significantly contribute to understand the complex plasmonic phenomena of circular dichroism.[55]

4. CONCLUSION

In summary, we have demonstrated a new strategy to achieve hybrid micelles encapsulated with well-ordered NRs. Binary polymer brushes on NRs surface create additional void spaces to accommodate sufficient conformational freedom for the matrix polymers close to the NRs surface.[56] This significantly improves the stable dispersion of the NRs in polymer matrix. Cylindrical micelles can direct NRs assembly into end-to-end

dx.doi.org/10.1021/ma400115z | Macromolecules 2013, 46, 2241−2248

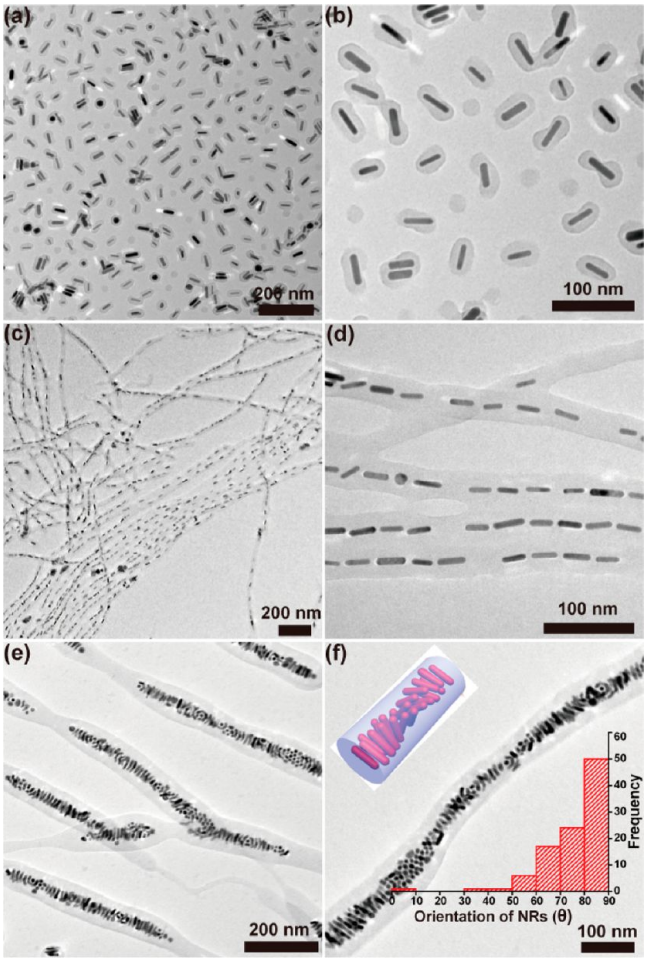

Figure 7. Bright-field TEM images of hybrid micelles formed from: (a, b) PS_{20k}-*b*-$P4VP_{17k}(PDP)_{1.0}$; (c, d) PS_{51k}-*b*-$P4VP_{17k}$ $(PDP)_{2.0}$; (e, f) PS_{110k}-*b*-$P4VP_{107k}$ $(PDP)_{1.0}$ encapsulated of NRs (content: ~ 27 vol %) (diameter: 7 nm; length: 29 nm). The NRs were grafted with mixed PS brushes (PS_{2k}:PS_{12k} = 1:1). Upper-left inset in part f is the cartoon showing the arrangement of NRs in the cylinders while the lower-right inset represents the histogram showing the orientation of the NRs.

nanostring or side-by-side hexagonal arrangement with a twist along the cylinder under cylindrical 2D confinement. Moreover, the orientation and length of NRs string can be easily tailored by varying loading content of NRs. These hybrid nanostructures may find potential applications in the area of optical device, drug delivery, catalysis, sensors, and biodiagnostic. We expect that our approach can be further extended to NRs with different functionalities or NPs with different shapes. Further work is ongoing to fully understand the mechanism of the wetting behavior of length mismatch and the orientation of NRs under the 2D confinement with the possibility of forming helical arrangement of the NRs.

■ ASSOCIATED CONTENT

Supporting Information

Additional tables and figures, including estimation of grafting density and volume fraction of gold NRs, NR orientation, histograms showing the length of the NRs strings distribution, UV−vis spectra of the Au NRs, and TEM and SEM images of spherical and cylindrical hybrid micelles. This material is available free of charge via the Internet at http://pubs.acs.org.

■ AUTHOR INFORMATION

Corresponding Author

*E-mail: jtzhu@mail.hust.edu.cn (J.Z.), znie@umd.edu (Z.N.).

Notes

The authors declare no competing financial interest.

■ ACKNOWLEDGMENTS

J.Z. gratefully acknowledges funding provided by National Basic Research Program of China (973 program, 2012CB812500 and 2012CB932500), the National Natural Science Foundation of China (51173056 and 91127046), Excellent Youth Foundation of Hubei Scientific Committee (2012FFA008) and Program of Chutian Scholars in Hubei Province. J.Z. thanks HUST Analytical and Testing Center for the TEM measurements. Z.N. acknowledges the support of startup funds and the Research and Scholarship Award (RASA) from University of Maryland. M.-H.L. acknowledges the support of the National Basic Research Program of China (Grant No. 2012CB921503). We also acknowledge the support of the Maryland NanoCenter and its NispLab. The NispLab is supported in part by the NSF as a MRSEC Shared Experimental Facilities.

■ REFERENCES

(1) Grzelczak, M.; Vermant, J.; Furst, E. M.; Liz-Marzan, L. M. *ACS Nano* **2010**, *4*, 3591.
(2) Zhang, H.; Liu, Y.; Yao, D.; Yang, B. *Chem. Soc. Rev.* **2012**, *41*, 6066.
(3) Langner, K. M.; Sevink, G. J. A. *Soft Matter* **2012**, *8*, 5102.
(4) Kao, J.; Thorkelsson, K.; Bai, P.; Rancatore, B. J.; Xu, T. *Chem. Soc. Rev.* **2012**, DOI: 10.1039/C2CS35375J.
(5) Jones, M. R.; Osberg, K. D.; Macfarlane, R. J.; Langille, M. R.; Mirkin, C. A. *Chem. Rev.* **2011**, *111*, 3736.
(6) Nie, Z.; Petukhova, A.; Kumacheva, E. *Nat. Nanotechnol.* **2010**, *5*, 15.
(7) Vigderman, L.; Khanal, B. P.; Zubarev, E. R. *Adv. Mater.* **2012**, *24*, 4811.
(8) Huynh, W. U.; Dittmer, J. J.; Alivisatos, A. P. *Science* **2002**, *295*, 2425.
(9) Chen, H.; Shao, L.; Q., Q.; Wang, J. *Chem. Soc. Rev.* **2013**, DOI: 10.1039/C2CS35367A.
(10) Liu, Z.; Huang, H.; He, T. *Small* **2013**, *9*, 505.
(11) Umadevi, S.; Feng, X.; Hegmann, T. *Adv. Funct. Mater.* **2012**, DOI: 10.1002/adfm. 201202727.
(12) Murphy, C. J.; Orendorff, C. J. *Adv. Mater.* **2005**, *17*, 2173.
(13) Perez-Juste, J.; Rodriguez-Gonzalez, B.; Mulvaney, P.; Liz-Marzan, L. M. *Adv. Funct. Mater.* **2005**, *15*, 1065.
(14) Zhang, C. L.; Lv, K. P.; Cong, H. P.; Yu, S. H. *Small* **2012**, *8*, 647.
(15) Wang, T.; Zhuang, J.; Lynch, J.; Chen, O.; Wang, Z.; Wang, Z.; LaMontagne, D.; Wu, H.; Wang, Z.; Cao, Y. C. *Science* **2012**, *338*, 358.
(16) Hore, M. J.; Composto, R. J. *ACS Nano* **2010**, *4*, 6941.
(17) Hore, M. J.; Frischknecht, L.; Composto, R. J. *ACS Macro Lett.* **2012**, *1*, 115.
(18) Nepal, D.; Onses, M. S.; Park, K.; Jespersen, M.; Thode, C. J.; Nealey, P. F.; Vaia, R. A. *ACS Nano* **2012**, *6*, 5693.
(19) Zhang, Q.; Gupta, S.; Emrick, T.; Russell, T. P. *J. Am. Chem. Soc.* **2006**, *128*, 3898.
(20) Ploshnik, E.; Salant, A.; Banin, U.; Shenhar, R. *Adv. Mater.* **2010**, *22*, 2774.
(21) Deshmukh, R. D.; Liu, Y.; Composto, R. J. *Nano Lett.* **2007**, *7*, 3662.
(22) Son, J. G.; Bae, W. K.; Kang, H.; Nealey, P. F.; Char, K. *ACS Nano* **2009**, *3*, 3927.
(23) Thorkelsson, K.; Mastroianni, A. J.; Ercius, P.; Xu, T. *Nano Lett.* **2012**, *12*, 498.

(24) Kumar, S. K.; Krishnamoorti, R. *Annu. Rev. Chem. Biomol. Eng.* **2010**, *1*, 37.
(25) Peng, G. *Science* **2000**, *288*, 1802.
(26) Frischknecht, A. L. *J. Chem. Phys.* **2008**, *128*, 224902.
(27) Trombly, D. M.; Ganesan, V. *J. Chem. Phys.* **2010**, *133*, 154904.
(28) Kim, J.; Green, P. F. *Macromolecules* **2010**, *43*, 1524.
(29) Zhao, B.; Zhu, L. *Macromolecules* **2009**, *42*, 9369.
(30) Edgecombe, S. R.; Gardiner, J. M. G.; Matsen, M. W. *Macromolecules* **2002**, *35*, 6475.
(31) Gao, B.; Arya, G.; Tao, A. R. *Nat. Nanotechnol.* **2012**, *7*, 433.
(32) Nikoobakht, B.; El-Sayed, M. A. *Chem. Mater.* **2003**, *10*, 1957.
(33) Ni, W.; Kou, X.; Yang, Z.; Wang, J. *ACS Nano* **2008**, *2*, 677.
(34) Li, Y.; Yu, D.; Dai, L.; Urbas, A.; Li, Q. *Langmuir* **2011**, *27*, 98.
(35) Li, W. K.; Liu, S. Q.; Deng, R. H.; Zhu, J. T. *Angew. Chem., Int. Ed.* **2011**, *50*, 5865.
(36) Nie, Z.; Fava, D.; Kumacheva, E.; Zou, S.; Walker, G. C.; Rubinstein, M. *Nat. Mater.* **2007**, *6*, 609.
(37) Zhu, J. T.; Zhao, J. C.; Liao, Y. G.; Jiang, W. J. *J. Polym. Sci., Part B: Polym. Phys.* **2005**, *43*, 2874.
(38) Zhu, J. T.; Ferrer, N.; Hayward, R. C. *Soft Matter* **2009**, *5*, 2471.
(39) Nie, Z.; Fava, D.; Rubinstein, M.; Kumacheva, E. *J. Am. Chem. Soc.* **2008**, *130*, 3683.
(40) Hickey, R. J.; Sanchez-Gaytan, B. L.; Cui, W.; Composto, R. J.; Fryd, M.; Wayland, B. B.; Park, S. J. *Small* **2010**, *6*, 48.
(41) He, L.; Zhang, L.; Xia, A.; Liang, H. *J. Chem. Phys.* **2009**, *130*, 144907.
(42) Chen, K.; Ma, Y.-Q. *J. Chem. Phys.* **2002**, *116*, 7783.
(43) Liu, K.; Nie, Z.; Zhao, N.; Li, W.; Rubinstein, M.; Kumacheva, E. *Science* **2010**, *329*, 197.
(44) Fava, D.; Nie, Z.; Winnik, M. A.; Kumacheva, E. *Adv. Mater.* **2008**, *20*, 4318.
(45) Lee, A.; Andrade, G. F.; Ahmed, A.; Souza, M. L.; Coombs, N.; Tumarkin, E.; Liu, K.; Gordon, R.; Brolo, A. G.; Kumacheva, E. *J. Am. Chem. Soc.* **2011**, *133*, 7563.
(46) Funston, A. M.; Novo, C.; Davis, T. J.; Mulvaney, P. *Nano Lett.* **2009**, *9*, 1651.
(47) Zijlstra, P.; Chon, J. W.; Gu, M. *Nature* **2009**, *459*, 410.
(48) Bockstaller, M. R.; Mickiewicz, R. A.; Thomas, E. L. *Adv. Mater.* **2005**, *11*, 1331.
(49) de Gennes, P.- G. *Scaling Concepts in Polymer Physics*; Cornell University Press: Ithaca, NY, 1979.
(50) Pryamitsyn, V.; Ganesan, V. *Macromolecules* **2006**, *39*, 8499.
(51) Horsch, M. A.; Zhang, Z.; Glotzer, S. C. *Phys. Rev. Lett.* **2005**, *95*, 056105.
(52) Horsch, M. A.; Zhang, Z. L.; Glotzer, S. C. *Soft Matter* **2010**, *5*, 945.
(53) Keys, A. S.; Iacovella, C. R.; Glotzer, S. C. *Annu. Rev. Condens. Matter Phys.* **2011**, *2*, 263.
(54) Ye, X.; Jin, L.; Caglayan, H.; Chen, J.; Xing, G.; Zheng, C.; Doan-Nguyen, V.; Kang, Y.; Engheta, N.; Kagan, C. R.; Murray, C. B. *ACS Nano* **2012**, *6*, 2804.
(55) Grzelczak, M.; Sanchez-Iglesias, A.; Mezerji, H. H.; Bals, S.; Perez-Juste, J.; Liz-Marzan, L. M. *Nano Lett.* **2012**, *12*, 4380.
(56) Fischer, S.; Salcher, A.; Kornowski, A.; Weller, H.; Forster, S. *Angew. Chem., Int. Ed.* **2011**, *50*, 7811.